Automated Detection of Posterior Tibial Slope on X-Ray Images Using VGG19

Showkat A. Dar[1], Alaa A. ELnazer[2,†], Snehal Rathi[3], Mohammad Nadeem Khalid[4,*], Aurchana[5], Divya Tirva[6], Showkat A. Bhat[7], Shabaan Ali[4] and Aafaq A. Rather[8]

[1]*Department of Computer Science and Engineering, GITAM University, Bangalore Campus-561203, India*

[2]*Department of Marketing, College of Business, Imam Mohammad Ibn Saud Islamic University (IMSIU), Riyadh 11432, Saudi Arabia*

[3]*Department of Computer Engineering, Vishwakarma Institute of Technology, Pune, India*

[4]*EMET Department, Abu Dhabi Polytechnic, Abu Dhabi, UAE*

[5]*Department of Computer Science and Engineering, Chennai Institute of Technology, Chennai, India*

[6]*Department of Chemical Engineering, Marwadi University, Rajkot-360003, India*

[7]*Symbiosis School of Economics, Symbiosis International (Deemed University), Pune, India*

[8]*Symbiosis Statistical Institute, Symbiosis International (Deemed University), Pune, India*

Abstract: Elderly and overweight individuals are particularly vulnerable to developing muscle weakness and joint pain as a result of osteoarthritis (OA). This degenerative joint condition often affects the ligaments and primarily damages the cartilage. Healthy cartilage, being smooth and elastic, enables bones to glide effortlessly over one another, providing stability and preventing friction between bone surfaces. When this protective tissue deteriorates partially or completely, it results in painful stiffness and discomfort caused by direct bone contact. The diagnosis of osteoarthritis typically involves a combination of clinical assessment and diagnostic imaging techniques such as X-rays or MRI scans. The present study focuses on utilising advanced image-based feature extraction methods for the identification and classification of knee osteoarthritis. This approach aims to enhance diagnostic accuracy by improving the differentiation of structural changes observed in medical images.

Keywords: Convolutional Neural Networks (CNNs), Deep learning, Machine learning, VGG-19 architecture, Image analysis, Pattern recognition.

1. INTRODUCTION

Just before distinguishing and separating the knee joints from the X-ray images and for a lot of computerized programming strategies of large datasets can be used. In terms of this detected midpoint, with reference to it, template matching is proposed for automatic detection of knee joints together with its surrounding region which is then extracted as region of interest (ROI); however, such methods give poor accuracy on large datasets. Therefore, we need to improve this by automatically localizing the knees from the X-ray image. At this stage in chapter two, localized knee region will be diagnosed whether normal or abnormal level of cartilage depreciation has been diagnosed. Otsu method was used in initial attempt to localize knees on X-ray images while HOG features were used for feature extraction; after which these features were classified using SVM and ANN Patternnet Classifiers – two different machine learning classifiers were employed for classification

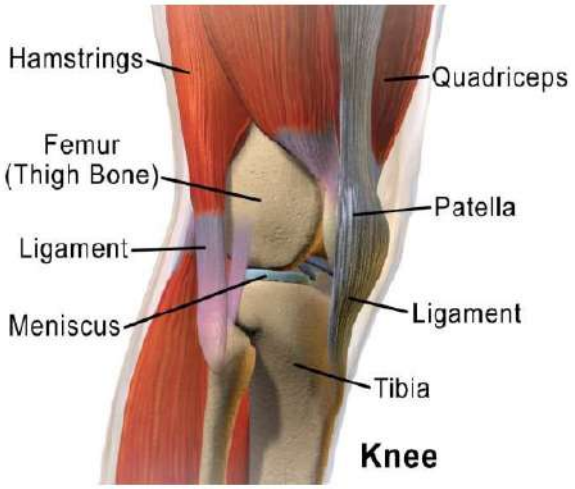

Figure 1: Normal knee Structure.

The human body has the largest and strongest knee joint. It is primarily made of bones, cartilage, ligaments and tendons. These are the patella or kneecap, tibia which is the upper end of shinbone and femur which is

*Address correspondence to this author at the EMET Department, Abu Dhabi Polytechnic, Abu Dhabi, UAE; E-mail: er.nkhalid@gmail.com

†E-mail: aaelnazer@imamu.edu.sa

the lower end of thighbone. A person's knee also has synovial fluid which lubricates this tissue as well as reduces friction during movements because articular cartilages are slippery tissues that cover where three bones meet at the joints enabling individuals to bend or straighten their knees without feeling any pain.

Two rubbery tough shock absorbers known as menisci lie between femur and tibia bone. They help in absorbing shocks so that the joint remains stable while still providing cushioning effect too. The synovial The thin layer of lining that surrounds the knee joint creates a lubricating fluid to reduce the rubbing of these components together when moving.

The condition known as osteoarthritis causes the knee joint's cartilage to deteriorate. As a result, there is less room for bones to rub against one another, which results in discomfort and inflammation. Furthermore, it causes excruciating bone spurs and, over time, progressively worsens pain.

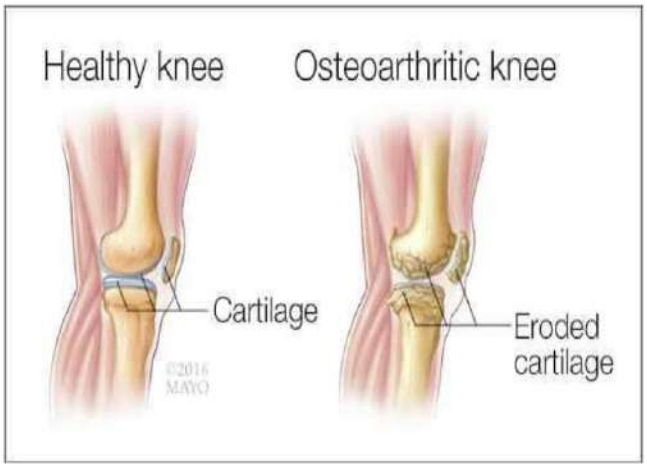

Figure 2: Normal and abnormal knee joint structures.

2. BACKGROUND LITERATURE

Fahri Emre *et al*. [1] performed a thorough postoperative knee function assessment and range of motion was done to determine the effect of sagittal alignment on surgical results. The results emphasize the necessity of incorporating both medial and lateral tibial slopes in the preoperative planning stage of knee arthroplasty. This detailed method of understanding the biomechanics of the joint guarantees a broader, more integrative consideration of the biomechanics of the joint, subsequently resulting in better surgery outcomes and postoperative knee function. Through the consideration of both components of tibial slope, surgeons can make their interventions patient-tailored to maximize alignment and thus contribute to the success of knee arthroplasty operations. The article promotes a precise and patient-specific surgical planning methodology to ensure optimal results in the restoration of the knee joint.

Hassa *et al*. [2] took it upon itself to exclude individuals with primary knee joint diseases and those who had undergone previous knee surgery or fractures in their joint. Out of 89 patients enrolled, 11 were excluded due to having proximal tibia fractures and six others due to their knee replacements appearing deviant on CT scans from what they ought to. This rigorous patient selection ensures that everyone is alike in nature and therefore the results are reliable as it eliminates possibilities of mistake through confounders and also limits research to just a single group that suits the existing inquiry in regards to health care delivery.

Sathya Sabina Muthu *et al*. [3] proposed a method involves cross-sectional design, which took place within one year from April 2020 through March 2021. The study was done at the Department of Radiodiagnosis and Imaging, located at KS Hegde Hospital in Mangaluru, Karnataka, India. The period covered included a thorough analysis of the set parameters within a given timeframe, providing a snapshot of the characteristics of the population at a given time. The selection of the Department of Radiodiagnosis and Imaging as the research site reflects an emphasis on sophisticated imaging methods and sophistication in analyzing the variables of interest. The location in Karnataka, India, serves as background to the local appropriateness of the results of the study.

Li Tong *et al*. [4] 1257 X-ray images were reviewed with the Picture Archiving and Communication System (PACS) in a retrospective review. The anterior tibial cortex was utilized as a means of measuring posterior tibial slope (PTS). Consistency among measurements was evaluated by way of inter- and intra-class correlation coefficients that ascertain the degree to which two sets correlate mathematically with each other; this ensures data gathered is consistent. Large numbers of x rays may be obtained to be retrieved and analyzed in a short span of time since PACS is used; thus it becomes feasible to incorporate all types of cases depicting various kinds of variation in slopes at the back end of tibia while conducting the phase of investigation in order to obtain effective results. This step-by-step approach used here reflects prudence used by researchers during the collection of data regarding PTSs.

Yoshiaki Hiranaka *et al*. [5] conducted with the use of X-rays to calculate knee alignment in single-leg standing. It incorporated the extension angle of the knee and the posterior tibial slope (PTS). It also examined the amount of forward tilt of the femoral and tibial shafts. They basically sought to know whether there was interdependence between those measurements and PTS, something that would enable us to know what impacts our knees in this particular position. By considering all these elements in combination it will provide us with a clearer insight regarding what occurs when an individual places weight on his leg and stands up with only one foot under him such that we may further research such complicated relation ships with varying aspects like PTS and other factors underlying alignment in weight bearing joints.

3. PROPOSED SYSTEM

3.1. Imaging Tests (X-Ray)

An X-Ray can show every bone in the body and is helpful in differentiating between arthritis types.

Joint space narrowing, bone changes, and osteophyte formation are among the things that can be seen on an X-Ray.

3.2. MRI & CT

Sometimes, to evaluate the bone and soft tissues of the knee, it may be necessary to use magnetic resonance imaging (MRI) or computed tomography (CT) scan images.

3.3. Image Processing Over X-RAY Images

Certainly, X-ray images are one of the oldest ways of detecting bones abnormality. It is a member of electromagnetic waves class of radiations. X-ray imaging takes pictures of inner part body. The photos show parts of body in different shades of black and white. This is because different tissues absorb different amounts of radiation. Bones appear white since calcium absorbs x-ray most. Less is absorbed in fat and other soft tissues hence they appear dark while lungs look dark because air absorbs the least. Image processing techniques over X-Ray images for better analysing output of medical imaging systems to get benefit analyse symptoms patients more easily. Partitioning bone structure from other regions such as muscle and background are very important yet difficult tasks within bone x-ray imaging.

Segmenting the area of bone helped find region interest (ROI) and check for crack, fracture, bone mineral density (BMD) and deformation.

The suggested architecture expands on previous X-ray analysis deep learning frameworks. The authors describe an automated CNN-based method that integrates preprocessing, segmentation, and classification modules to increase diagnostic accuracy in musculoskeletal imaging in their related patented work, "Fracture Classification System in X-Ray Images and Method Employed Thereof" [10].

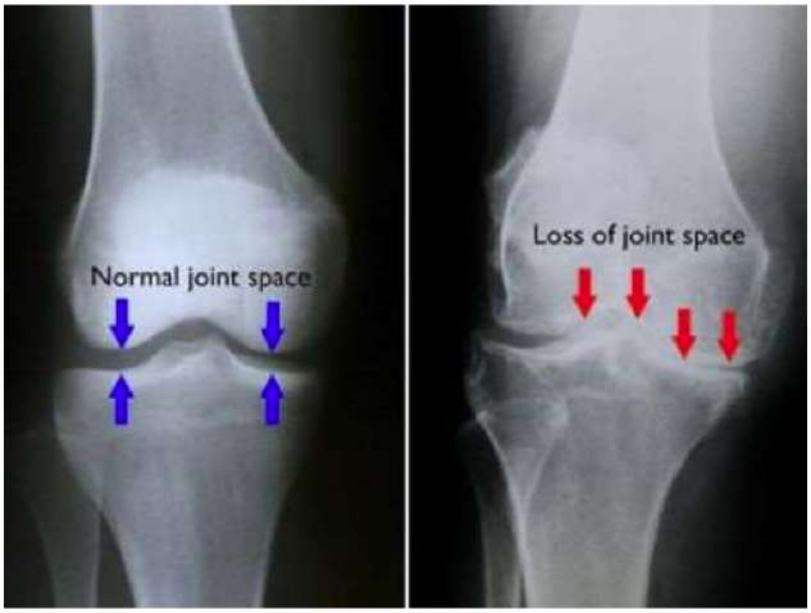

Figure 3: (**Left**) In this x-ray of a normal knee, (**Right**) severe loss of joint space.

3.4. Classification Process

(In general, classification using any kind of classifier) Training and testing are the two phases in the classifier construction process. Sub-steps can be added to these phases for more organization.

1. Training

a. Pre-processing: This stage prepares the data to be used in training by...

b. Feature extraction: This method of reducing the amount of data involves removing pertinent information, which often yields a vector of scalar values. (In order to estimate distance, we also need to Normalize the characteristics!)

c. Model Estimation: For each class of training data, a model (often statistical) must be estimated from the finite collection of feature vectors.

2. Examination

a. Pre-processing

b. Feature extraction

c. Classification: Locate the most similar match between feature vectors and the different models. One may make use of a distance measure.

VGG is an established better vision model architecture (Visual Geometry Group). VGG19, a modified version of VGG16 that is deeper for image recognition due to more layers with convolution operation, has been used in this study. Deep learning-based convolutional networks such as VGG19 have shown remarkable accuracy in various medical image classification problems, including disease diagnosis and structural feature extraction [21, 22, 26]. that is deeper for image recognition due to more layers with convolution operation, has been used in this study. It consists of many convolution layers followed by a

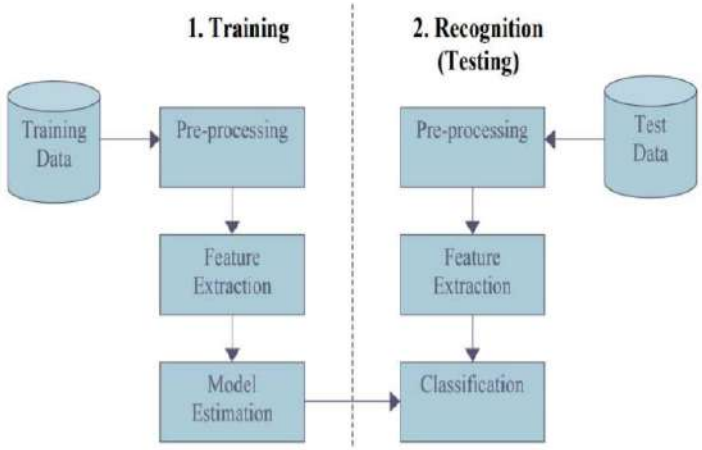

Figure 4: Pattern Classification Process.

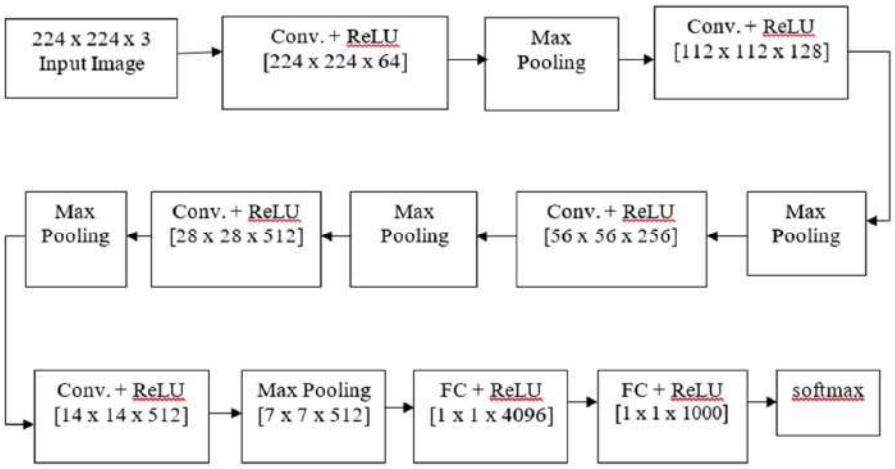

Figure 5: Dimension of CNN-VGG19.

pooling layer then another flattening layer before three fully connected layers and lastly a softmax layer according to Garcia *et al*. (2017). See Figure **5** for details about this 19-layer network model design.

The VGG19 model takes a 224×224 RGB image as an input. There are five convolutional blocks in the model, the first one having three convolution layers with 64 filters and the second one having two convolution layers with 128 filters. Block 3 applies 256 filters over 4 convolutional layers.

Both blocks 4 and 5 include 4 convolution layers and 512 filters, respectively. After every block except for the last one there is a max-pooling layer following the final convolution layer with a filter size of two by two, stride of 2 ×2 and activation function ReLU. After the flattening step we obtain 25088 feature values from that stage onwards.

Three Fully-Connected (FC) layers follow a stack of convolutional layers; while each of the first two has got its channels increased by four times compared to previous ones (which were equal for all classes), third FC performs classification itself being provided with additional thousand channels besides usual four thousand assigned per class):

Table 1: Dimension of CNN-VGG19

Layer no.	Layer	Input Size
1	Conv x 2	3x224x224
2	Pool	64x224x224
3	Conv x 2	64x112x112
4	Pool	128x112x112
5	Conv x 4	128x56x56
6	Pool	256x56x56
7	Conv x 4	256x28x28
8	Pool	512x28x28
9	Conv x 4	512x14x14
10	Pool	512x14x14
11	Fc	25088
12	Fc	4096
13	Fc	1000
14	Softmax	5

3.5. CNN Components

Convolution (CONV), Non-Linearity (RELU), Pooling or Sub Sampling (POOL) and Classification (FC) are the major building blocks of Convolutional Neural Networks.

3.5.1. Convolution

The convolutional layer is the basic building block of CNN. Similar CNN architectures have been successfully applied in biomedical applications such as Alzheimer's disease detection, lung cancer screening, and facial authentication, demonstrating the robustness and adaptability of CNNs for healthcare diagnostics [21, 23, 26]. It does most of the computational work in the network. Convolution aims to extract features of an object. In other words, a convolutional network for image and video processing will learn specific patterns within an image (frame) and be able to recognize it wherever it appears in the image. Essentially, convolution is a mathematical operation (in particular element-wise multiplication), which by applying a learnt kernel /patches / filter(f) expresses shape or some other feature of an image. The kernel is a small matrix where its size and values determine how much effect should be done during the transformation part of convolution process (Liu *et al*., 2018). This process involves placing Kernel Matrix over every pixel in image, multiplying each value from Kernel by corresponding pixel it is on top of then summing up all these multiplied results returning this as new value for center pixel. As shown below, this step will be performed throughout whole picture.

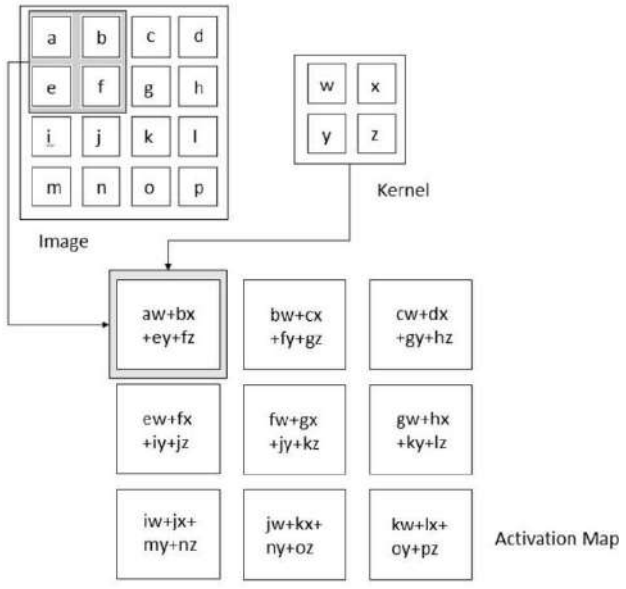

Figure 6: Convolution process.

This process will analyze the entire image of size 3×3 (or) 5×5 by multiplying it with a filter. The resultant of element-wise multiplication is called feature map. After convolution, the size of image reduces. Each layer of convolution operation has different kernel values and also different dimension of kernel, which

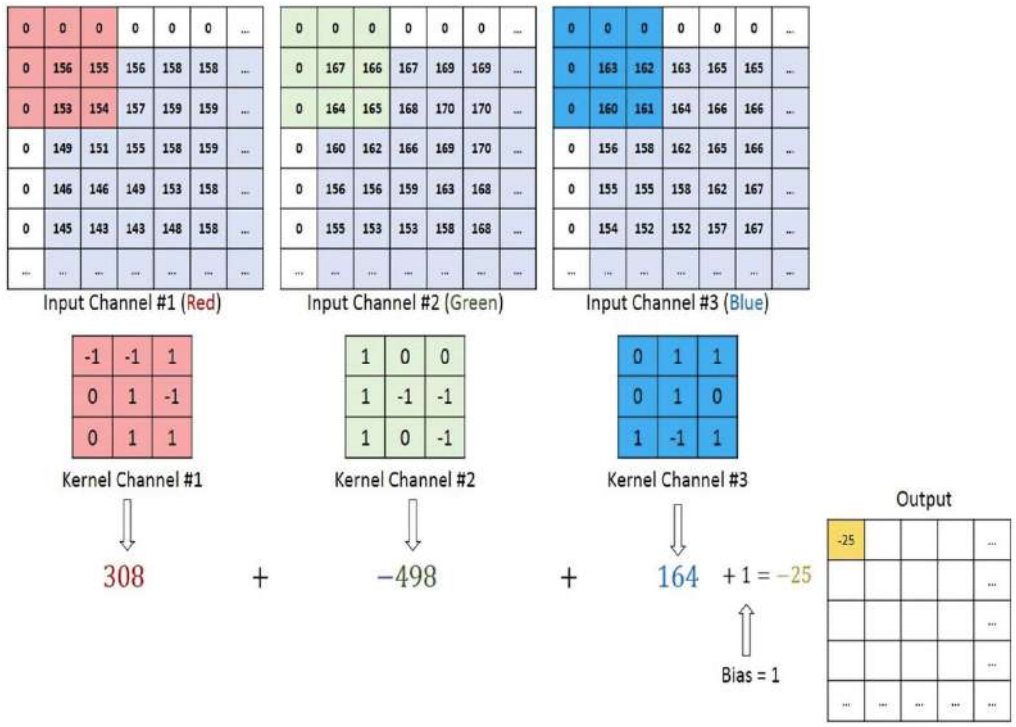

Figure 7: Convolution process using Filters.

are used for different feature extraction and enhancement such as edge detection, embossing, rotation, blurring etc. During forward pass, Kernel creates an image representation of that receptive region by sliding across height and breadth of an image. This results in the creation of an activation map, a two-dimensional representation of a picture that displays the kernel's response at each spatial location within the image. The amount of kernel sliding is called a stride.

The previous figure shows how convolution works. The kernels are much smaller spatially than an image but deeper in terms of depth. Meaning if the image has size of three (RGB) channels then kernel height and width (spatial sizes) will be small but depth will go all the way to three channels.

3.5.2. Padding Effect

In center there will be one window where a 3×3 grid can be displayed if the image has a 5×5 features map and a 3×3 filter. The final feature map will have a size of 3x3, shrinking by two tiles. Padding should be done to make sure that output dimensions match input dimensions. This is achieved by adding rows and columns on either side of the matrix; it's called padding. With this, every input tile can be fitted centered by convolution. Convolved features are governed by three parameters:

3.5.2.1. Depth

This determines how many filters are used in the convolution process. For instance, if the depth is 1, it means that just one filter is being applied, yet in most cases, multiple filters are being used. The actions carried out in a scenario involving three filters are depicted in the image below.

3.5.2.2. Stride

This shows how many "pixels move" between two slices. Strides of 1 will make windows move by one pixel at a time whereas if stride was set to equal two then windows would jump over two pixels each time. Smaller feature maps occur when stride increases.

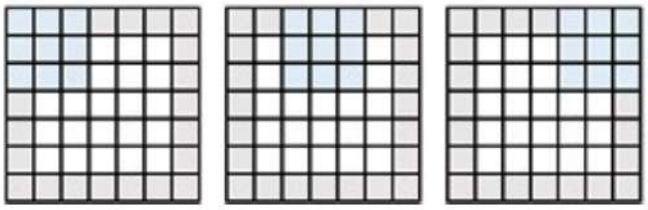

Figure 8: Stride Process.

1. Zero-padding: By zero-padding the input feature maps with corresponding numbers of rows and columns, a padding is done.

The next following is how to calculate the dimension of an output image from a convolution layer.

- Output height = (Input height + padding height top + padding height bottom - kernel height) / (stride height) + 1
- Output width = (Output width + padding width right + padding width left - kernel width) / (stride width) + 1

The parameters that are involved in Convolution are:

- Input dimensions: height, width, batch size and number of channels
- Kernel height and Kernel width
- Stride height and stride width
- Padding height top, Padding height bottom
- Padding width right, Padding width left

3.5.3. Non Linearity Layer

The explanation why non-linearity layers are often placed right after a convolutional layer is because convolution is a linear operation while pictures are not. There are many different types of non-linear operations, but some of the most well-known are:

3.5.3.1. Sigmoid

The sigmoid function takes on the form σ(κ) = 1/(1+e^κ) mathematically. It maps any real number to a range between zero and one. However, it suffers from such an undesirable property that its gradient almost vanishes whenever the activation is at either tail. A too small local gradient in backpropagation would “kill” the gradient altogether. Moreover, if only positive input has been received by a neuron, then the output of sigmoid will have both negative and positive values inducing a zigzag pattern into weight gradients.

3.5.3.2. Tanh

This squashes numbers (Tanh) into the range -1 through 1 inclusive. Similar to Sigmoid neurons this activation saturates but it outputs are zero-centered.

$$tanh(x) = \frac{e^{k} - e^{-k}}{e^{k} + e^{-k}} \quad (1)$$

3.5.3.3. ReLU

Convnet usually uses Rectified Linear Unit (ReLU) as activation function, which has gained much popularity in recent years. ReLu computes this function,

$$y(x) = \max(0,x) \quad (2)$$

Alternatively speaking, the activation is simply zero threshold. It is six times faster than sigmoid or tanh because of being more reliable. However, one disadvantage with ReLU is its brittleness during training; it might be updated so that never gets another update from passing large gradients over it. But we can overcome this by setting up right learning rate.

3.5.4. Pooling Operation

Reducing the input image's width and height is the goal of the pooling process. These steps are performed to reduce the amount of computation in an operation. In order to prevent overfitting, the network also reduces dimensionality which means fewer weights need to be computed. There are different types of pooling functions: average, min and max. Max Pooling – chooses the largest pixel value from each batch. Min Pooling – chooses the smallest pixel value from each batch.

Additionally, Average Pooling – selects the mean value for each pixel across a batch is used as well. Size and stride must be specified when doing pooling activities. The most popular application of max pooling is when we take the feature map's maximum value. while taking minimum value is called min and likewise average can be taken into account depending upon what we want or need from our model's architecture.

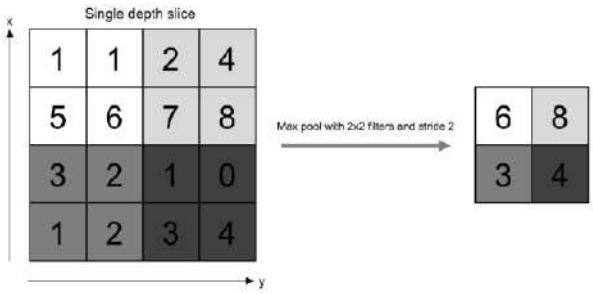

Figure 9: Pooling Process.

This is max pooling where it takes maximum values from feature map throughout its size but this method decreases image size significantly so pay attention below: The 4x4 “pooling” process on a feature map will look at four submatrices and return their highest value. After finding maximums in 2×2 array pools shift these windows by two pixels down then do same left right till end of row then next row until all rows have been covered, for example if first sub-matrix [1,1,5,6], pooling would give us max which is six because this operation dramatically shrinks down feature maps sizes.

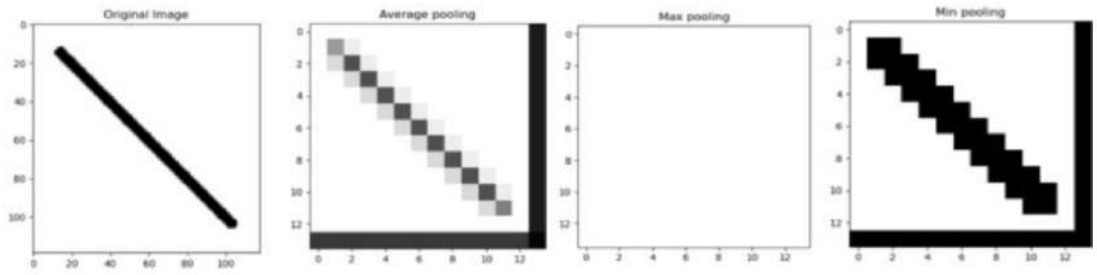

Figure 10: Min pooling in white background and black object.

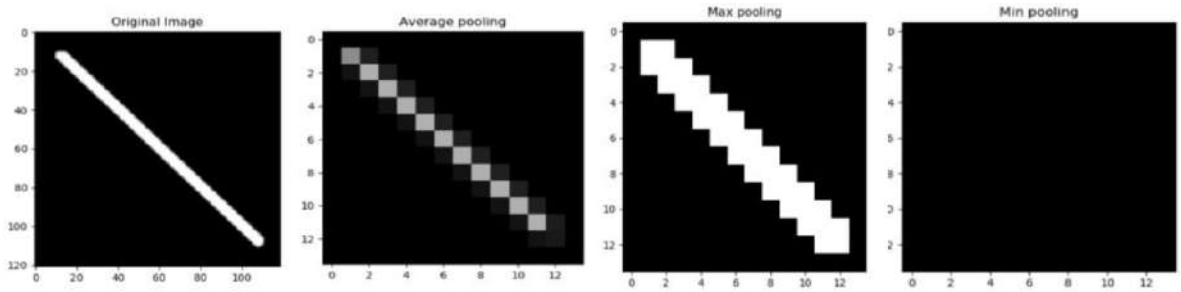

Figure 11: Max pooling in black background and white object.

Generally, it can't be stated that there are measures of pool that stand out in terms of performance. Data is what informs the choice of pooling operation. Consequently, some sharp features may be lost in an image smoothed by average pooling method. Max pooling highlights the bright pixels of the image.

3.5.5. Fully Connected Layers

The best tag for describing the object is predicted by a fully connected layer. The Fully Connected Layer (Hidden Layer) is the last layer of the Convolutional Neural Network (Yamashita *et al*., 2018). Deep learning models that employ such fully connected layers, in combination with GRU and LSTM variants, have been reported to yield enhanced pattern recognition and classification performance in medical and biometric systems [22, 25] is the last layer of the Convolutional Neural Network (Yamashita *et al*., 2018). This layer is comprised of an Affine function and a Non-Linear function (Sigmoid, TanH, ReLu).

To “flatten” them into one-dimensional vectors that can be used as input in the next stage, the flatten layer of the fully linked layer takes output from earlier layers. First, data comes to Flatten Layer from which it later goes to Non- Linear function after passing through Affine Function. One FC or hidden layer consists of one Affine function and one non-linear function. It uses weights to predict appropriate label(s). These layers may be added multiple times depending on how deep we want our classification to go. Sigmoid or Softmax functions are used at the end for determining probability distribution across all classes in final set after routing through last hidden layer.

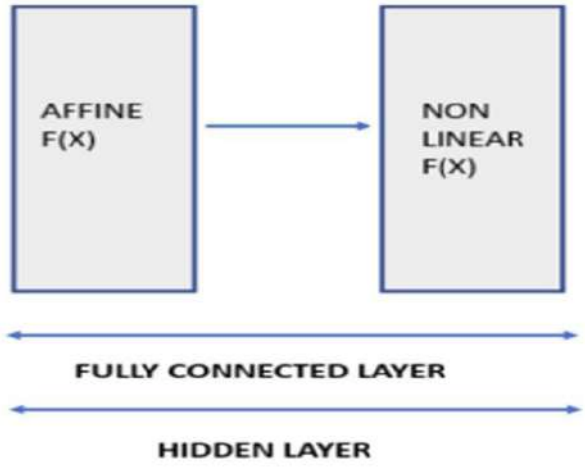

Figure 12: Affine function.

3.5.6. Training and Validation

Any application that analyzes the performance of the trained models must include both training and testing. Consequently, Similar validation strategies using CNN-based models have been adopted across various AI-driven diagnostic systems to ensure model reliability and generalization in unseen medical data [24-32]. Consequently, the trained model receives the 1680 testing samples. The confusion matrix (for mistake) contains one of the most significant categorization ideas. This matrix is a table that shows

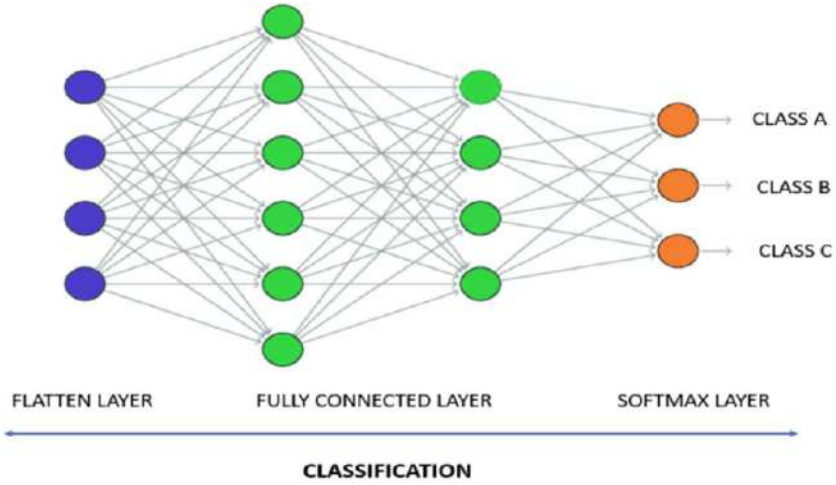

Figure 13: Fully Connected Layer.

how well an algorithm performs and can be used to create other matrices. The instances that truly belong to are represented by the matrices' column. The term comes from the matrix's ability to clearly display whether the system is confusing two classes. This matrix counts the instances that are successfully classified (true) or wrongly labeled (false) for each class and has two categories (such as positive and negative).

An instance is now considered successful if it is accurately anticipated to be a true positive (TP) or true negative (TN).

3.5.7. Predicted Class and True Class

Confusion matrix represents classification results using four outcomes-True Positive (TP), False Positive (FP), False Negative (FN), and True Negative (TN) to evaluate model's accuracy. The evaluation of True Positive Rate (TPR) and False Positive Rate (FPR).

$$\text{TPR} = \frac{TP}{TP+FN} \quad (3)$$

$$\text{FPR} = \frac{FP}{FP+TN} \quad (4)$$

The total number of users who were correctly identified using the suggested method is known as the true TP. FP is the total number of users that the suggested method mistakenly recognized.

Then Precision and Recall can be calculated as:

$$\text{Precision (P)} = \frac{TP}{TP+FP} \quad (5)$$

$$\text{Recall (R)} = \frac{TP}{TP+FN} \quad (6)$$

Then erroneous detection F-measure can be calculated as:

$$\text{F-measure} = \frac{2\times P\times R}{P+R} \quad (7)$$

where, P and R are precision and recall.

4. PERFORMANCE MATRIX

Performance matrix is used as a tool for evaluating how well a model performs on different categories or classes. Such evaluation matrices have also been adopted in deep learning research for other medical imaging domains to compare classification accuracy, sensitivity, and precision among AI-driven models [21, 22] as a tool for evaluating how well a model performs on different categories or classes. In this case, the model is VGG-19, and the classes probably represent various types of medical images that the model classifies (Normal, OA-1, OA-2, OA-3, OA-4). The matrix would contain selected relevant KPIs to assess the performance of the model. Typical options include precision, recall and F1- score. Precision shows what proportion of positive predictions are true positives. Recall indicates how well the model can identify all relevant instances of a class. F1-score is a number that takes the harmonic mean of precision and recall thereby giving a balanced view overall. Every class (Normal, OA-1 etc.) should be assigned its own row within this table-like structure called 'matrix'.

Each KPI (precision, recall, F1-score) would have its own column. The corresponding values for each class and KPI would be populated in the cells of the matrix. You can include an additional row for the overall performance metrics (average precision, recall, F1-score) if relevant.

Table 2: Overall Performance of VGG19

	Precision	Recall	F-Score
Normal	83	100	91
OA-1	95	82	88
OA-2	0.85	100	92
OA-3	100	90	95
OA-4	92	100	96
Accuracy			92

Utilize the performance matrix to assess the model's performance across classes. High recall implies the model is retrieving the most relevant examples while high precision implies the model is making few errors. F1-score gives you a combined view. You will be able to see the model's benefits and drawbacks for different classes and also determine if it is acceptable for your purpose by examining these metrics.

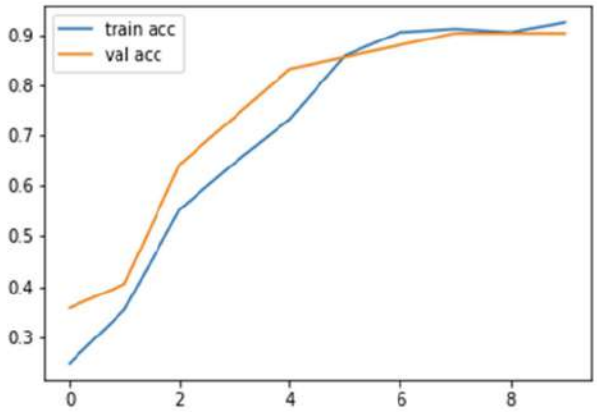

Figure 14: Training Accuracy.

In addition to locating strengths and weaknesses, the performance matrix can help to inform developmental activities. For instance, if a class, OA-3, has a low F1-score due to having a low recall value, it implies that the model may be missing many relevant OA-3 cases.

This might mean that more training data specific to OA-3 is required in order to help the model recognise these cases, or it might indicate that different image pre-processing techniques should be tried, or modifications made to the model architecture to improve sensitivity for this specific class.

In this way, the performance matrix provides some very useful insight into how to target improvements in a model, based on viewing class-level performance differences. Also, when reflecting on the overall effectiveness of a model, it is wise to consider aspects of the study beyond the matrix as well. For instance, the choice of KPIs can often lead to different interpretations.

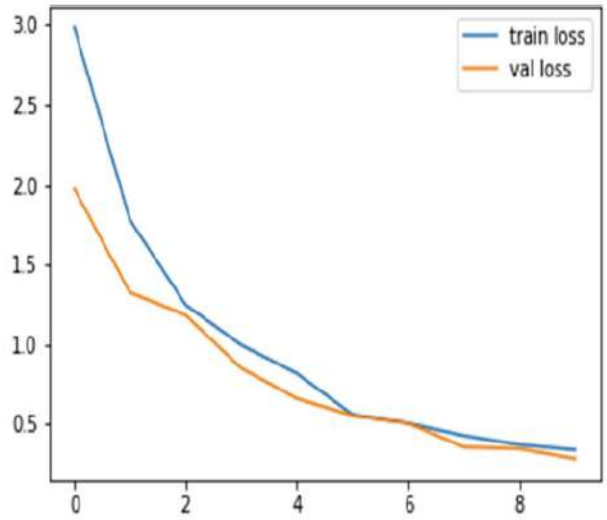

Figure 15: Training L.

5. CONCLUSION

Our study demonstrates that a VGG19-inspired 1D CNN provides a reliable, efficient and low-cost method for detecting posterior tibial slope abnormalities. adaptability, this AI-driven approach enhances diagnostic precision and represents a significant advancement in musculoskeletal healthcare and orthopedic clinical practice. This is consistent with similar CNN-based diagnostic frameworks reported in recent literature on Alzheimer's disease detection, face authentication, and automated lung cancer diagnosis [21, 22, 26] in musculoskeletal healthcare and orthopedic clinical practice.

REFERENCES

[1] Emre F, Bozkurt M. Lateral Tibial Slope Should Be Considered When Planning Medial Unicompartmental Knee Arthroplasty. Journal of Clinical Practice and Research 2023. https://doi.org/10.14744/cpr.2023.58077

[2] Hassa E, Uyanik SA, Kosehan D, Alic T. CT-based analysis of posterior tibial slope in a Turkish population sample: A retrospective observational study. Research Gate Journal 2023. https://doi.org/10.1097/MD.0000000000033452

[3] Muthu SS, Shrikrishna U, Ravichandran K. Evaluation of Posterior Tibial Slope for Anterior Cruciate Ligament Tear and Meniscal Tear: A Cross-sectional Study. Journal of Clinical and Diagnostic Research 2023. https://doi.org/10.7860/JCDR/2023/58727.17268

[4] Tong L, Xue S, Chen X, Fang R. Artificial intelligence-based detection of posterior tibial slope on X-ray images of unicompartmental knee arthroplasty patients. Research gate Journal 2023. https://doi.org/10.1016/j.jrras.2023.100615

[5] Hiranaka Y, Muratsu H, Tsubosaka M, Matsumoto T, Maruo A, Miya H, Kuroda R, Matsushita T. Influence of posterior tibial slope on sagittal knee alignment with comparing contralateral knees of anterior cruciate ligament injured patients to healthy knees. Research Gate Journal 2022. https://doi.org/10.1038/s41598-022-18442-y

[6] Supreeth S, Al Barwani A, Al Manei, K, Al Ghanami, Suwailim S, Saseendar K, Vijay K. Is Posterior Tibial Slope and Mechanism of Failure Crucial for an Anatomically Reconstructed Primary Hamstring Graft Anterior Cruciate Ligament? Journal of Arthroscopy and Joint Surgery 2022. https://doi.org/10.4103/jajs.jajs_87_22

[7] Meier M-P, Hochrein Y, Saul D, Seitz M-T, Klockner FS, Lehmann W, Hawellek T. Morphological Analysis of the Tibial Slope in 720 Adult Knee Joints. Research Gate Journal 2022. https://doi.org/10.3390/diagnostics12061346

[8] Cruz CA, Mannino BJ, Pike A, Thoma D, Lindell K, Kerbel YE, Bottoni CR, McCadden A, Lopez AJ. Increased posterior tibial slope is an independent risk actor of anterior cruciate ligament reconstruction graft rupture irrespective of graft choice. Journal of ISAKOS 2022. https://doi.org/10.1016/j.jisako.2022.04.002

[9] Fares A, Horteur C, Al Ezz MA, Hardy A, Rubens-Duval B, Karam K, Gaulin B, Pailhe R. Posterior tibial slope (PTS) 210 degrees isa risk factor for further anterior cruciate ligament (ACL) injurvy; BMI is not. European Journal of Orthopedic Surgery and Traumatology 2023. https://doi.org/10.1007/s00590-022-03406-9

Dar SA, MC, Indhumathi R, Sardar TH. Fracture classification system in X-ray images and method employed thereof. Indian Patent IN202441069005A 2024.

[10] Chen Y, Ding J, Dai S, Yang J, Wang M, Tian T, Deng X, Li B, Cheng G, Liu J. Radiographic measurement of the posterior tibial slopein normal Chinese adults: a retrospective cohort study. Research Gate Journal 2022. https://doi.org/10.1186/s12891-022-05319-4

[11] Korthaus A, Krause M, Pagenstert G, Warncke M, Brembach F, Karl-Heinz F, Kolb JP. Tibial slope in the posterolateral quadrant with and without ACL injury. PubMed Journal 2021. https://doi.org/10.1007/s00402-021-04298-w

[12] Faschingbauer M. Posterior Tibial Slope: The "Unknown Size" of the Knee Joint. Anthroscopy Journal 2021; 2020: 10.024.

[13] Matas BM, Barberà IC, Marsico S, Claramunt AA, Torres-Claramunt R, López AS. Importance of Posterior Tibial Slope, Medial Tibial Plateau Slope and Lateral Tibial Plateau Slope in Anterior Cruciate Ligament Injury. Scientific Research Publishing Journal 2021. https://doi.org/10.4236/ojo.2021.119022

[14] Alsowaigh M, Arafah MA, Alharbi SK, AlSultan O, Alshahrani A, Al Hulaibi FH, Bin Nasser A. Posterior tibial slope measurement among Saudi population. Medcrave Online Journal 2021. https://doi.org/10.15406/mojor.2021.13.00549

[15] Hecker A, Lerch TD, Egli RJ, Liechti EF, Klenke FM. The EOS 3D imaging system reliably measures posterior tibial slope. Journal of Orthopaedic and Research 2021. https://doi.org/10.1186/s13018-021-02529-9

[16] Kacmaz IE, Topkaya Y, Basa CD, Zhamilov V, Er A, Reisoglu A, Ekizoglu O. Posterior tibial slope of the knee measured on X-rays in a Turkish population. Research Gate Journal 2020. https://doi.org/10.1007/s00276-020-02430-w

[17] Jahn R, Cooper JD, Juhan T, Kang HP, Bolia IK, Gamradt SC, Hatch GF, Weber AE. Reliability of Plain Radiographs Versus Magnetic Resonance Imaging to Measure Tibial Slope in Sports Medicine Patients: Can They Be Used Interchangeably? Sage Journals 2021. https://doi.org/10.1177/23259671211033882

[18] Veizi E, Fırat A, Tecimel O, Epni Ş, Subaşı İÖ, Kılıçarslan K. The Change in Posterior Tibial Slope After Cementless Unicondylar Knee Arthroplasty. PubMed Journal 2020; 2020.12.041

[19] Kunal K, Kumar R. Radiographic evaluation of posterior tibial slope in ACL deficient Indian patients. Research Gate Journal 2020; 10.18203

[20] Dar SA, *et al*. Improving Alzheimer's Disease Detection with Transfer Learning. Int J Stat Med Res 2025; 14: 403-415. https://doi.org/10.6000/1929-6029.2025.14.39

[21] Dar SA, Palanivel S, Geetha MK, Balasubramanian M. Mouth Image Based Person Authentication Using DWLSTM and GRU. Inf Sci Lett 2022; 11(3): 853-862. https://doi.org/10.18576/isl/110317

[22] Dar SA, Palanivel S. Performance Evaluation of Convolutional Neural Networks (CNNs) And VGG on Real-Time Face Recognition System. Adv Sci Technol Eng Syst J 2021; 6(2): 956-964. https://doi.org/10.25046/aj0602109

[23] Dar SA, Palanivel S. Real Time Face Authentication System Using Stacked Deep Auto Encoder for Facial Reconstruction. Int J Thin Film Sci Technol 2022; 11(1): 73-82. https://doi.org/10.18576/ijtfst/110109

[24] Dar SA, PS. Real-Time Face Authentication Using Denoised Autoencoder (DAE) for Mobile Devices 2022; 21(6): 163-176. https://doi.org/10.4018/978-1-7998-9795-8.ch011

[25] Ayadi W, *et al*. AI-Powered CNN Model for Automated Lung Cancer Diagnosis in Medical Imaging. Int J Stat Med Res 2025; 14: 616-625. https://doi.org/10.6000/1929-6029.2025.14.58

[26] Ibrahim H, Mahmoud M, Ahmad M, Mandouh R. Different Approaches for Outlier Detection in Life Testing Scenarios. Computational Journal of Mathematical and Statistical Sciences 2024; 3(1): 203-227. https://doi.org/10.21608/cjmss.2024.254148.1033

[27] Onyekwere C, Nwankwo C, Obulezi O, Ezeilo C. The feature-value paradox: Unsupervised discovery of strategic archetypes in the smartphone market using machine learning. Journal of Artificial Intelligence in Engineering Practice 2025; 2(2): 65-72. https://doi.org/10.21608/jaiep.2025.420689.1024

[28] Raihen MN, Hossain MI, Chellamuthu V. Predicting clinical outcomes in liver cirrhosis using machine learning and data balancing technique. Computational Journal of Mathematical and Statistical Sciences 2025; 4(2): 664-696. https://doi.org/10.21608/cjmss.2025.397747.1213

[29] Shalaby Y, Embark A. A predictive model for climate change using advanced machine learning algorithms in Egypt. Journal of Artificial Intelligence in Engineering Practice 2025; 2(2): 1-21. https://doi.org/10.21608/jaiep.2025.415474.1020

[30] Nnaekwe K, Ani E, Obieke V, Okechukwu C, Usman A, Othman M. Forecasting seasonal rainfall with time series,

machine learning and deep learning. Innovation in Computer and Data Sciences 2025; 1(1): 51-65. https://doi.org/10.64389/icds.2025.01127

[31] Almetwally EM, Elbatal I, Elgarhy M, Kamel AR. Implications of machine learning techniques for prediction of motor health disorders in Saudi Arabia. Alexandria Engineering Journal 2025; 27: 1193-1208. https://doi.org/10.1016/j.aej.2025.07.015

Received on 27-09-2025 Accepted on 29-10-2025 Published on 21-11-2025

https://doi.org/10.6000/1929-6029.2025.14.63